

# The Use of Shell Elements for the Analysis of Large Strain Response

Charles C. Rankin<sup>1</sup>  
Rhombus Consultants Group, Inc.  
Palo Alto, CA 94303

Last year we demonstrated that Element-Independent Corotation based on polar decomposition at the element centroid permits analysis of systems undergoing large-strain response with standard off-the-shelf elements originally designed for moderate strains. This capability has implications for a wide variety of problems of special importance to aerospace structures, many of which consist of thin members best modeled by shell elements, where a plane-stress and linear through-the-thickness strain variation approximate quite closely the actual response. Given the motivation to minimize problem size and computer resource requirements, it is very desirable to have shell elements that can handle large membrane strains and at the same time faithfully reproduce plane stress response in the presence of severe thinning of the shell cross section. In this paper, we shall present our strategy for computing results presented last year for shells. We shall demonstrate superior accuracy and convergence properties for large-strain response for a variety of standard shell elements with and without transverse shear deformation.

## Nomenclature

$\mathbf{F}, \mathbf{U}$	=	deformation gradient and right stretch tensor, respectively
$\boldsymbol{\varepsilon}$	=	strain
$C_b, K_b$	=	Mooney-Rivlin material constants and bulk modulus, respectively
$(\bullet)_{,ij}$	=	derivative of indicated quantity with respect to engineering strain component $ij$
$\lambda_i$	=	$i$ 'th eigenvalue of $\mathbf{U}$ .
$J$	=	determinant of $\mathbf{U}$
$\mathbf{Q}$	=	matrix of eigenvectors of $\mathbf{U}$ with each eigenvector a <i>column</i> in $\mathbf{Q}$ .
$\boldsymbol{\Omega}, \boldsymbol{\omega}$	=	spin of eigenvectors $\mathbf{Q}$
$S$	=	stress conjugate to a given strain measure
$e$	=	square of stretch eigenvalues
$\bar{H}_{ij}^{(kl)}$	=	variation of strain component ( $ij$ ) with respect to a unit variation of tensor strain component ( $kl$ )
$v_i$	=	the third component $i$ 'th eigenvector of $\mathbf{U}$ (component along the shell director)
$p$	=	hydrostatic pressure required to enforce volume and stress constraints

## I. Introduction

Last year<sup>1</sup> we demonstrated that Element-Independent Corotation<sup>2-4</sup> based on polar decomposition at the element centroid permits analysis of systems undergoing large-strain response with standard off-the-shelf elements originally designed for moderate strains. In that work, we showed that with only modest changes to existing corotation software, a displacement field is presented to the finite element kernels that is irrotational (pure straining) at the centroid, and approximates pure strain over the rest of the element. We also demonstrated that strain based on a linear small-displacement formulation approaches Biot strain in the limit of a fine grid, which provides an excellent starting point for the implantation of large-strain material models. We followed that presentation with

---

<sup>1</sup> Consulting Specialist, Associate Fellow AIAA

several examples of large strain response for a material based on a Mooney-Rivlin potential function. What we did not do in that paper is to derive the material models as they apply to the shell and solid elements used for these examples. Although for solid elements, the derivation is based on standard methods<sup>5</sup>, the use of shell elements allowing transverse shear deformation poses special challenges to the generation of the consistent tangent material stiffness matrix. In this paper we shall cover the development of the material model in the form of a UMAT for both solid and shell finite elements. We shall also show that for plane stress shell analysis, the volume constraint can be introduced directly, simplifying the implementation considerably. Finally, we shall demonstrate the method with examples.

## II. Theoretical Development

### A. Strain measures

As covered previously<sup>1</sup>, strains derived from a linear strain-displacement relationship applied to displacements based on the updated Element-Independent Corotation methodology approach Biot strains in the limit of fine discretization. We achieve such a displacement field by first straining the body and afterwards by rotating the element rigidly until the nodal displacements match the system displacement field. The operation is identical to polar decomposition at the centroid, hence its association with Biot strain.<sup>5-7</sup> Several of the elements also have the ability to generate Green's strain. For this reason, we shall be covering both Biot and Green strain measures:

$$\begin{aligned}\boldsymbol{\varepsilon}^G &\equiv \frac{1}{2}(\mathbf{U}^T \mathbf{U} - \mathbf{I}) = \frac{1}{2}(\mathbf{F}^T \mathbf{F} - \mathbf{I}) \\ \boldsymbol{\varepsilon}^B &\equiv \mathbf{U} - \mathbf{I} \\ \mathbf{F} &= \mathbf{R}\mathbf{U}\end{aligned}\tag{1}$$

In this set of equations,  $\mathbf{F}$  is the displacement gradient,  $\mathbf{I}$  is the identity matrix of order 3,  $\mathbf{R}$  is an orthogonal rotation matrix, and  $\mathbf{U}$  is the right stretch tensor. The superscripts  $G$  and  $B$  refer to Green and Biot strains, respectively.

### B. Mooney Rivlin Potential Function

We have chosen the Mooney-Rivlin<sup>5</sup> potential function to illustrate our large strain response:

$$\varphi_d = C_1(\lambda_1^2 + \lambda_2^2 + \lambda_3^2 - 3J^{\frac{2}{3}}) + C_2(\lambda_1^{-2} + \lambda_2^{-2} + \lambda_3^{-2} - 3J^{-\frac{2}{3}}) + \frac{1}{2}K_b(J - 1)^2\tag{2}$$

Here,  $C_1$  and  $C_2$  and  $K_b$  are material constants, the  $\lambda_i$  are the principal stretches, and

$$J = \det(\mathbf{F}) = \det(\mathbf{U}) = \lambda_1 \lambda_2 \lambda_3\tag{3}$$

represents the fractional volume change for the point in question. This form of the potential function applies also to compressible materials; however, for most situations including those treated here, the bulk modulus  $K_b$  is large compared to the other material response constants.

### C. Procedure for computing the stress—solids

The stress field for solid elements is the easiest to derive because all six stresses participate, and no explicit constraints are imposed. It can be shown by standard methods that the stress is the derivative of the potential function as a function of the principal stretches. Stresses derived in this manner are expressed in the principal coordinate system, defined by the eigenvalue problem that diagonalizes the stretch tensor  $\mathbf{U}$ :

$$\mathbf{UQ} - \mathbf{Q}\mathbf{\Lambda} = 0$$

$$\mathbf{\Lambda} = \begin{bmatrix} \lambda_1 & & \\ & \lambda_2 & \\ & & \lambda_3 \end{bmatrix} \quad (4)$$

$\mathbf{Q}$  is an orthogonal transformation. In this principal strain system, the stresses are:

$$S_{ii}^B = 2 \left[ C_1 \left( \lambda_i - J^{\frac{2}{3}} \lambda_i^{-1} \right) - C_2 \left( \lambda_i^{-3} - J^{-\frac{2}{3}} \lambda_i^{-1} \right) \right] + K_b J(J-1) / \lambda_i \quad (5)$$

Here we have the stresses conjugate to Biot strains. The reader will notice that they are diagonal in this coordinate frame. For Green's strain, we have

$$S_{ii}^G = 2C_1 \left( 1 - J^{\frac{2}{3}} e_i^{-1} \right) - 2C_2 \left( e_i^{-2} - J^{-\frac{2}{3}} e_i^{-1} \right) + K_b J(J-1) / e_i \quad (6)$$

In this case,

$$e_i = \lambda_i^2 \quad (7)$$

The procedure for computing stresses given strains in a reference frame is to first compute the principal strains and their directions  $\mathbf{Q}$ . The stresses computed by Eq. (5) or (6) are then transformed back to the reference frame and returned to element kernels. These computations are easily performed in a "UMAT" or user written constitutive processor that has available to it (among other things) indicators as to what the strain measure is, the strains in the reference frame, and the material constants.

#### D. Eigenvalue and eigenvector derivatives

The other quantity that is required for a nonlinear material is the material tangent modulus. In contrast to the very simple procedure for computing stresses, additional terms come into play for the tangent modulus because of the rotation of the principal strain directions (eigenvectors) as a function of perturbations to the input strains. Even though the methods for deriving the tangent modulus for solids are off the shelf and appear very often in the literature (for example in Ref. 5), it is instructive to repeat some of this development here, partly because it is difficult to find all the needed information in one place. We begin by restating Eq. (4) as follows:

$$\mathbf{\Lambda} = \mathbf{Q}^T \mathbf{UQ} \quad (8)$$

If we take the variation of Eq. (8) we obtain

$$\delta\mathbf{\Lambda} = (\delta\mathbf{Q})^T \mathbf{UQ} + \mathbf{Q}^T \delta\mathbf{UQ} + \mathbf{Q}^T \mathbf{U} \delta\mathbf{Q} \quad (9)$$

where the variations of the stretch tensor are assumed to be independent. The left hand side of Eq. (9) is diagonal, whereas the matrices on the right hand side are in general full. One will also notice that because

$$\mathbf{Q}^T \mathbf{Q} = \mathbf{I}$$

$$(\delta\mathbf{Q})^T \mathbf{Q} + \mathbf{Q}^T \delta\mathbf{Q} = \mathbf{0} = \delta\mathbf{\Omega}^T + \delta\mathbf{\Omega} \quad (10)$$

$$\delta\mathbf{\Omega} \equiv \mathbf{Q}^T \delta\mathbf{Q}$$

the “spin” matrix  $\delta\mathbf{\Omega}$  is antisymmetric and has only three independent components. If we substitute (10) into (9), we obtain

$$\begin{aligned}\delta\mathbf{\Lambda} &= -\delta\mathbf{\Omega}\mathbf{Q}^T\mathbf{U}\mathbf{Q} + \mathbf{Q}^T\delta\mathbf{U}\mathbf{Q} + \mathbf{Q}^T\mathbf{U}\mathbf{Q}\delta\mathbf{\Omega} \\ &= -\delta\mathbf{\Omega}\mathbf{\Lambda} + \mathbf{\Lambda}\delta\mathbf{\Omega} + \mathbf{Q}^T\delta\mathbf{U}\mathbf{Q}\end{aligned}\quad (11)$$

Given the definition of  $\mathbf{\Lambda}$ , the only solution for  $\mathbf{\Omega}$  is as follows:

$$\delta\omega_1 = \frac{\delta\bar{U}_{23}}{\lambda_2 - \lambda_3}; \quad \delta\omega_2 = \frac{\delta\bar{U}_{31}}{\lambda_3 - \lambda_1}; \quad \delta\omega_3 = \frac{\delta\bar{U}_{12}}{\lambda_1 - \lambda_2}\quad (12)$$

where we have defined

$$\delta\bar{\mathbf{U}} \equiv \mathbf{Q}^T\delta\mathbf{U}\mathbf{Q}\quad (13)$$

The quantity on the left hand side of (13) is just the variation of the tensor strains expressed in the principal system coordinates. Note that these variations are in general *not* diagonal. Finally, we have

$$\delta\mathbf{\Omega} \equiv \begin{bmatrix} 0 & -\delta\omega_3 & \delta\omega_2 \\ \delta\omega_3 & 0 & -\delta\omega_1 \\ -\delta\omega_2 & \delta\omega_1 & 0 \end{bmatrix}\quad (14)$$

We also have for the diagonal term the following relationship:

$$\delta\lambda_i = \delta\bar{U}_{ii}\quad (15)$$

Eq. (15) is what permits us to transform the strains into the principal system, compute the stresses by a simple derivative, and transform the result back: *the variation of the eigenvalue is identical to the variation of their respective diagonal component in the stretch tensor*. The explicit form for the transformation of the stresses from the principal system back to the reference system comes from the inverse of Eq. (8):

$$\mathbf{S} = \mathbf{Q}\mathbf{S}_d\mathbf{Q}^T\quad (16)$$

where  $\mathbf{S}_d$  are in diagonal form in the principal strain system. If we wish to compute the tangent modular matrix, we need to take the variation of (16); it will soon be apparent that the rotation of the principal directions gives rise to off-diagonal shear terms. The variation of Eq. (16) yields

$$\begin{aligned}\delta\mathbf{S} &= \delta\mathbf{Q}\mathbf{S}_d\mathbf{Q}^T + \mathbf{Q}\delta\mathbf{S}_d\mathbf{Q}^T + \mathbf{Q}\mathbf{S}_d(\delta\mathbf{Q})^T \\ &= \mathbf{Q}[\delta\mathbf{\Omega}\mathbf{S}_d - \mathbf{S}_d\delta\mathbf{\Omega} + \delta\mathbf{S}_d]\mathbf{Q}^T \\ &= \mathbf{Q}\delta\bar{\mathbf{S}}\mathbf{Q}^T \\ \delta\bar{\mathbf{S}} &= (\delta\mathbf{\Omega}\mathbf{S}_d - \mathbf{S}_d\delta\mathbf{\Omega}) + \sum_{i=1}^3 \mathbf{S}_{d,\lambda_i}\delta\lambda_i\end{aligned}\quad (17)$$

The new off-diagonal terms come from the spin of the eigenvectors<sup>5</sup>. The  $d$  subscript is used here to refer to the diagonal stresses, and its variation is with respect to the principal stretches.

### E. Tangent modulus for solids

Eq. (17) provides all the necessary information to compute the tangent stiffness for solids. The last term in Eq. (17) is very straightforward, with a simple differentiation of (6) yielding for Biot strain the following:

$$\begin{aligned} S_{ii,ii}^B &= 2C_1 \left( 1 + \frac{1}{3} J^{\frac{2}{3}} \lambda_i^{-2} \right) + 2C_2 \left( 3\lambda_i^{-4} - \frac{5}{3} J^{-\frac{2}{3}} \lambda_i^{-2} \right) + K_b J^2 \lambda_i^{-2} \\ S_{ii,ij}^B &= -\frac{4}{3\lambda_i \lambda_j} \left( C_1 J^{\frac{2}{3}} + C_2 J^{-\frac{2}{3}} \right) + K_b (2J - 1) \lambda_k \end{aligned} \quad (18)$$

If we apply the first two terms in Eq. (17d) to the stresses from Eq. (6) we obtain the following additional terms:

$$S_{23,23}^B = \left[ C_1 + C_2 \frac{(\lambda_2^2 + \lambda_2 \lambda_3 + \lambda_3^2)}{(\lambda_2 \lambda_3)^3} \right] - \frac{1}{\lambda_2 \lambda_3} \left( \frac{1}{2} K_b J (J - 1) - C_1 J^{\frac{2}{3}} + C_2 J^{-\frac{2}{3}} \right) \quad (19)$$

There are two additional shear terms obtained by a cyclic permutation of the indices on  $\lambda$  and  $S^B$ . Please note that in this and all other equations, we use comma notation in the subscripts to indicate partial derivatives; for example, in Eq. (19) we mean the derivative of the shear term (23) with respect to strain component (23). There is a factor of one half in Eq. (19) because the tangent modulus here is defined in terms of engineering strains instead of tensor strains. One must pay particular attention to the second term in the first bracket of Eq. (19). Its explicit derivation goes as follows:

$$\delta \Omega \mathbf{S}_d - \mathbf{S}_d \delta \Omega = \begin{bmatrix} 0 & \delta \omega_3 (S_{11}^B - S_{22}^B) & \delta \omega_2 (S_{33}^B - S_{11}^B) \\ & 0 & \delta \omega_1 (S_{22}^B - S_{33}^B) \\ \text{Symm.} & & 0 \end{bmatrix} \quad (20)$$

In this equation, the change in shear stress component  $\delta S_{23}^B$  is equal to  $\delta \omega_1 (S_{22}^B - S_{33}^B)$ . The same applies to the other terms by a cyclic permutation of the indices; there are no other nonzero shear terms for the tangent modulus in the principal strain coordinate system. Now we make use of Eq. (12). When we substitute in the values for  $\delta \omega$ , we notice that explicit limits exist for the ratios of the type

$$\frac{\lambda_2^{-3} - \lambda_3^{-3}}{\lambda_2 - \lambda_3} = \frac{\lambda_2^2 + \lambda_2 \lambda_3 + \lambda_3^2}{(\lambda_2 \lambda_3)^3} \quad (21)$$

Limits like this will appear repeatedly in what follows, and there will never be a case where any tangent stiffness term does not possess a well-defined limit when one or more eigenvalues are equal. We shall henceforth present only the results of the limiting process in what follows for shells.

For Green's strain, we have the following nonzero tangent stiffness terms:

$$\begin{aligned}
S_{ii,ii}^G &= \frac{8}{e_i^2} \left( \frac{1}{3} C_1 J^{\frac{2}{3}} + C_2 \left[ e_i^{-1} - \frac{2}{3} J^{-\frac{2}{3}} \right] \right) + K_b J e_i^{-2} \\
S_{ii,jj}^G &= -\frac{4}{3e_i e_j} \left( C_1 J^{\frac{2}{3}} + C_2 J^{-\frac{2}{3}} \right) + K_b e_k (2 - 1/J)
\end{aligned} \tag{22}$$

The shear terms are

$$S_{23,23}^G = \frac{2}{e_2 e_3} \left[ C_1 J^{\frac{2}{3}} + C_2 \left( \frac{(e_2 + e_3)}{e_2 e_3} - J^{-\frac{2}{3}} \right) - \frac{1}{2} K_b J (J - 1) \right] \tag{23}$$

with the other shear terms given by a cyclic permutation of the indices on  $e$  and  $S^G$ . For the tangent modulus for either strain measure, one must transform it back into the reference frame using standard methods.

#### F. Shells without transverse shear deformation

One can easily extend the procedure described above for solids to plane stress analysis using shell elements without transverse shear deformation. In this case, we take  $J=1$  in Eq. (2) and eliminate the last term. It is then a simple matter to use the fact that the stress normal to the shell surface is zero to solve for the unknown hydrostatic pressure required to enforce the constraint  $J=1$ . The procedure is explained fully in Ref. 5 and will not be repeated here. The procedure involves computing the variations in the principal strain space and then transforming the result back, just as in solids. When there is no transverse shear, one of the principal directions remains normal to the shell, so the volume constraint is easy to apply. The resulting stresses are

$$\begin{aligned}
S_{11}^B &= 2C_1 (\lambda_1 - \lambda_1^{-3} \lambda_2^{-2}) + 2C_2 (\lambda_1 \lambda_2^2 - \lambda_1^{-3}) \\
S_{22}^B &= 2C_1 (\lambda_2 - \lambda_2^{-3} \lambda_1^{-2}) + 2C_2 (\lambda_2 \lambda_1^2 - \lambda_2^{-3})
\end{aligned} \tag{24}$$

for Biot strain and

$$\begin{aligned}
S_{11}^G &= 2C_1 (1 - e_1^{-2} e_2^{-1}) + 2C_2 (e_2 - e_1^{-2}) \\
S_{22}^G &= 2C_1 (1 - e_2^{-2} e_1^{-1}) + 2C_2 (e_1 - e_2^{-2})
\end{aligned} \tag{25}$$

for Green strain. The tangent modulus is similarly straightforward:

$$\begin{aligned}
S_{11,11}^B &= 2C_1 (1 + 3\lambda_1^{-4} \lambda_2^{-2}) + 2C_2 (\lambda_2^2 + 3\lambda_1^{-4}) \\
S_{22,22}^B &= 2C_1 (1 + 3\lambda_2^{-4} \lambda_1^{-2}) + 2C_2 (\lambda_1^2 + 3\lambda_2^{-4}) \\
S_{11,22}^B &= 4(C_1 \lambda_1^{-3} \lambda_2^{-3} + C_2 \lambda_1 \lambda_2) \\
S_{12,12}^B &= C_1 (1 + \lambda_2^{-3} \lambda_1^{-3}) + C_2 [(\lambda_1^2 + \lambda_1 \lambda_2 + \lambda_2^2) \lambda_2^{-3} \lambda_1^{-3} - \lambda_1 \lambda_2]
\end{aligned} \tag{26}$$

Again here, there is a factor of a half in the last term because here we are using engineering strains for the shear term. The Green's tangent modulus is also straightforward:

$$\begin{aligned}
S_{11,11}^G &= 8e_1^{-3}(C_1e_2^{-1} + C_2) \\
S_{22,22}^G &= 8e_2^{-3}(C_1e_1^{-1} + C_2) \\
S_{11,22}^G &= 4C_1e_1^{-2}e_2^{-2} + 4C_2 \\
S_{12,12}^G &= 2C_1e_1^{-2}e_2^{-2} + 2C_2[(e_1 + e_2)e_2^{-2}e_1^{-2} - 1]
\end{aligned} \tag{27}$$

### G. Shell elements with transverse shear deformation

Difficulties arise immediately when applying the results of the previous section to shells exhibiting transverse shear deformation. This is because the direction in which the “normal” stress is zero no longer is normal to the shell, but instead follows the *shell director* that rotates slightly away from the shell normal in response to shearing. Thus, all three principal strain directions can rotate, making the constraint of zero “director” stress expressed in the principal system a function of the principal strain eigenvectors. Explicitly, the zero stress constraint becomes

$$\begin{aligned}
0 &= \sum_{i=1}^3 Q_{3i}^2 S_{ii} = \sum_{i=1}^3 v_i^2 S_{ii} \\
v_i &\equiv Q_{3i}; \quad \sum_{i=1}^3 v_i^2 = 1
\end{aligned} \tag{28}$$

Here, we are assuming that the third component in each eigenvector  $i$  belongs originally to the shell normal in the undeformed state, an arrangement that is easy to achieve in practice. The last equation comes from the orthonormality of the eigenvectors. The requirement of zero stress along the director is found by differentiating the potential energy function with respect to the principal stretches and applying Eq. (28):

$$\begin{aligned}
S_{ii}^B &= 2(C_1\lambda_i - C_2\lambda_i^{-3}) - \frac{1}{\lambda_i} p \\
\sum_{i=1}^3 \frac{v_i^2}{\lambda_i} p &= 2 \sum_{i=1}^3 v_i^2 (C_1\lambda_i - C_2\lambda_i^{-3}) \\
Dp &= 2 \sum_{i=1}^3 v_i^2 (C_1\lambda_i - C_2\lambda_i^{-3}) \\
D &\equiv \sum_{i=1}^3 \frac{v_i^2}{\lambda_i}
\end{aligned} \tag{29}$$

The first equation in Eq. (29) is the general expression for the Biot stress expressed in the principal strain system. The new quantity  $p$  in Eq. (29) is the unknown hydrostatic pressure required to enforce the volume and zero stress constraints, which is solved by the second equation. The rationale for the definition of  $p$  is explained in Ref. 5 and will not be repeated here. The nonzero strain along the director comes from the requirement that  $J = 1$ :

$$\begin{vmatrix}
\varepsilon_{11} + 1 & \gamma_{12} / 2 & \gamma_{13} / 2 \\
\gamma_{12} / 2 & \varepsilon_{22} + 1 & \gamma_{23} / 2 \\
\gamma_{13} / 2 & \gamma_{23} / 2 & \varepsilon_{33} + 1
\end{vmatrix} = 1 \tag{30}$$

Here the strains are in their original system. The explicit solution for the strain in the third direction is

$$\begin{aligned}
b_i &\equiv \varepsilon_{ii} + 1; \quad B \equiv b_1 b_2 - \frac{1}{4} \gamma_{12}^2 \\
b_3 &= \frac{1 + \frac{1}{4} (b_1 \gamma_{23}^2 + b_2 \gamma_{13}^2 - \gamma_{12} \gamma_{23} \gamma_{13})}{B}
\end{aligned} \tag{31}$$

So far everything is quite straightforward. One first computes all six strains using the volume constraint expressed in Eqs. (30) and (31). One then solves for the principal directions, obtains the principal stretches, and obtains the stresses. Stresses are subsequently transformed back into the reference system.

#### H. The tangent modular matrix

It would appear that one could follow exactly the same procedure as for stresses to obtain the tangent modular material stiffness matrix. One would work as with solids and shells without transverse shear: solve for the normal strain, find the principal directions, and treat each variation in the principal system as independent. The result would be very similar to what we have done before.

Unfortunately, such a procedure fails miserably. The reason of course is that the strain variations are *not* independent. Whereas for shells without transverse shear maintain one principal direction along the normal that does not change as the structure deforms, the constraint in (28) depends on the third component of all three eigenvectors in a situation where their components along the shell normal *are* changing. For stress, this presents no problem, because the variation of the principal stresses in that system depends only on the diagonal members of the strain, and not the eigenvectors except for Eq. (29b) that is applied explicitly. Not so for the tangent modular matrix.

To obtain this stiffness, we must perform our variations in the original system, and then transform these variations into the principal strain system to compute the stiffness components. To begin the process, we first compute the variation of the normal strain (in the reference state that is normal to the shell) as a function of the other five strains. This comes from the differentiation of Eq. (31):

$$\begin{aligned}
\varepsilon_{33,11} &= \frac{1}{4B} (-4b_3 b_2 + \gamma_{23}^2); \quad \varepsilon_{33,22} = \frac{1}{4B} (-4b_1 b_3 + \gamma_{13}^2) \\
\varepsilon_{33,12} &= \frac{1}{4B} (2b_3 \lambda_{12} - \gamma_{23} \gamma_{13}); \quad \varepsilon_{33,23} = \frac{1}{4B} (2b_1 \lambda_{23} - \gamma_{13} \gamma_{12}) \\
\varepsilon_{33,13} &= \frac{1}{4B} (2b_2 \lambda_{13} - \gamma_{12} \gamma_{23}); \quad \gamma_{ij} = 2\varepsilon_{ij}, i \neq j
\end{aligned} \tag{32}$$

The variations for the shear terms are with respect to the *engineering* strains that are twice their tensor values. From Eq. (32) is clear that the variation of the normal strain is an explicit function of the other five strains. To obtain the stiffness, we take a *unit variation* of each of the five strains in turn and only then transform them into the principal strain system.

$$\begin{aligned}
\mathbf{H}^{(11)} &= \begin{bmatrix} 1 & 0 & 0 \\ 0 & 0 & 0 \\ 0 & 0 & \varepsilon_{33,11} \end{bmatrix}; \quad \mathbf{H}^{(22)} = \begin{bmatrix} 0 & 0 & 0 \\ 0 & 1 & 0 \\ 0 & 0 & \varepsilon_{33,22} \end{bmatrix} \\
\mathbf{H}^{(12)} &= \begin{bmatrix} 0 & 1/2 & 0 \\ 1/2 & 0 & 0 \\ 0 & 0 & \varepsilon_{33,12} \end{bmatrix}; \quad \mathbf{H}^{(23)} = \begin{bmatrix} 0 & 0 & 0 \\ 0 & 0 & 1/2 \\ 0 & 1/2 & \varepsilon_{33,23} \end{bmatrix}; \quad \mathbf{H}^{(13)} = \begin{bmatrix} 0 & 0 & 1/2 \\ 0 & 0 & 0 \\ 1/2 & 0 & \varepsilon_{33,13} \end{bmatrix}
\end{aligned} \tag{33}$$

In this equation, each matrix represents the variation of a particular independent strain component indicated by the superscript in parenthesis, with the new dependent term being the third diagonal term that comes from the volume constraint. The transformation of each strain variation into the principal strain system comes from Eq. (8):

$$\bar{\mathbf{H}}^{(ij)} = \mathbf{Q}^T \mathbf{H}^{(ij)} \mathbf{Q} \quad (34)$$

Because each of these matrices stem from unit variation of the labeled strain component, they can be substituted directly into Eq. (17) to get the corresponding variation in the stress. All of the stress variations computed in this manner apply to that particular component of strain labeled by the superscripts. When one arranges strains into a vector as is common practice for finite element analysis, these variations actually become a particular column in the tangent modular stiffness matrix.

We begin with the last term in Eq. (17) by taking the derivative of the stresses, including the pressure term as a function of the stretches and the eigenvectors. By the chain rule, the differentiation of the stresses (Eq. (28) becomes:

$$S_{ii,kl}^B = \sum_{j=1}^3 S_{ii,\lambda_j}^B \bar{H}_{jj}^{(kl)} + S_{ii,v}^B \quad (35)$$

The last term in Eq. (35) is the dependence of the stress on the third component  $v_i$  of each eigenvector  $i$ . It is straightforward to show that in the principal reference frame,

$$\begin{aligned} \mathbf{v}^T &\equiv [v_1 \quad v_2 \quad v_3] \\ \mathbf{v}_{,kl} &= \mathbf{v} \times \boldsymbol{\omega}^{(kl)} \\ \omega_1^{(kl)} &= \frac{\bar{H}_{23}^{(kl)}}{\lambda_2 - \lambda_3} \end{aligned} \quad (36)$$

The remaining terms for the spin are obtained from a cyclic permutation of the indices. These equations are valid because of the orthonormality of the eigenvectors and Eq. (12). Here the reader is reminded that the subscripts on  $\bar{H}$  refer to a particular component in that matrix, whereas the superscripts refer to the strain component being varied.

It would appear that the last relationship in Eq. (36) would present problems when the two stretches approach each other. Again, however, the limit exists. To see this, we examine Eq. (29b) that defines the pressure  $p$ . If we differentiate this, we are left with polynomials like this:

$$\begin{aligned} P &= v_1^2 \lambda_1^\alpha + v_2^2 \lambda_2^\alpha + v_3^2 \lambda_3^\alpha \\ P_{,kl} &= 2(v_1 v_{1,kl} + v_2 v_{2,kl} + v_3 v_{3,kl}) \end{aligned} \quad (37)$$

where  $\alpha$  is some positive or negative integer, and where we are taking the variation with respect to the eigenvector components. Written out, the cross product from Eq. (36b) expands to

$$\left[ \mathbf{v} \times \boldsymbol{\omega}^{(kl)} \right]^T = \left[ v_2 \omega_3^{(kl)} - v_3 \omega_2^{(kl)} \quad v_3 \omega_1^{(kl)} - v_1 \omega_3^{(kl)} \quad v_1 \omega_2^{(kl)} - v_2 \omega_1^{(kl)} \right] \quad (38)$$

We now apply Eq. (36c) to the derivative terms in Eq. (37b) to yield the following sequence of equations:

$$\begin{aligned} P_{,kl} &= 2v_1 (v_2 \omega_3^{(kl)} - v_3 \omega_2^{(kl)}) \lambda_1^\alpha + 2v_2 (v_3 \omega_1^{(kl)} - v_1 \omega_3^{(kl)}) \lambda_2^\alpha + 2v_3 (v_1 \omega_2^{(kl)} - v_2 \omega_1^{(kl)}) \lambda_3^\alpha \\ &= 2\omega_1^{(kl)} v_2 v_3 (\lambda_2^\alpha - \lambda_3^\alpha) + 2\omega_2^{(kl)} v_3 v_1 (\lambda_3^\alpha - \lambda_1^\alpha) + 2\omega_3^{(kl)} v_1 v_2 (\lambda_1^\alpha - \lambda_2^\alpha) \\ P_{,kl} &= 2\bar{H}_{23}^{(kl)} v_2 v_3 \frac{\lambda_2^\alpha - \lambda_3^\alpha}{\lambda_2^2 - \lambda_3^2} + 2\bar{H}_{31}^{(kl)} v_3 v_1 \frac{\lambda_3^\alpha - \lambda_1^\alpha}{\lambda_3^2 - \lambda_1^2} + 2\bar{H}_{12}^{(kl)} v_1 v_2 \frac{\lambda_1^\alpha - \lambda_2^\alpha}{\lambda_1^2 - \lambda_2^2} \end{aligned} \quad (39)$$

Clearly the limits are similar to Eq. (21), so that all expressions are well-defined.

We use Eq. (35) to obtain the derivatives of the stresses, as follows:

$$S_{ii,kl}^B = \bar{H}_{ii}^{(kl)} (2C_1 + 6C_2\lambda_i^{-4} + p\lambda_i^{-2}) - p_{,kl}\lambda_i^{-1} \quad (40)$$

The first term is the explicit derivative of the stresses with respect to the stretch  $\lambda_i$ , and the second term is the derivative of the pressure term. Only this latter term has dependence on the direction of the eigenvectors, where we shall be using Eq. (39c). To obtain the derivative of the pressure, we first rearrange the equation defining  $p$  (Eq. (29.b)) like this:

$$Dp = \Gamma; \quad D \equiv \sum_{i=1}^3 \frac{v_i^2}{\lambda_i}; \quad \Gamma \equiv 2 \sum_{i=1}^3 v_i^2 (C_1\lambda_i - C_2\lambda_i^{-3}) \quad (41)$$

The variation of  $p$  becomes

$$p_{,kl} = \frac{\Gamma_{,kl} - pD_{,kl}}{D} \quad (42)$$

Finally we compute the explicit derivatives and use Eq. (39) to obtain

$$\begin{aligned} \Gamma_{,kl} &= 2 \sum_{i=1}^3 v_i^2 \bar{H}_{ii}^{(kl)} (C_1 + 3C_2\lambda_i^{-4}) + 4 \sum_{i=1}^3 v_{i+1} v_{i+2} \bar{H}_{(i+1)(i+2)}^{(kl)} (C_1 + C_2\psi_{(i+1)(i+2)}) \\ \psi_{ij} &\equiv \frac{\lambda_i^2 + \lambda_i\lambda_j + \lambda_j^2}{(\lambda_i\lambda_j)^3}; \quad D_{,kl} = - \sum_{i=1}^3 \left[ v_i^2 \lambda_i^{-2} \bar{H}_{ii}^{(kl)} + 2v_{i+1} v_{i+2} \bar{H}_{(i+1)(i+2)}^{(kl)} \lambda_{i+1}^{-1} \lambda_{i+2}^{-1} \right] \end{aligned} \quad (43)$$

where we have taken the appropriate limits. The indices (subscripts) here cycle from 1 to 3 in a modular fashion; for example, if  $i=2$ ,  $i+1=3$  and  $i+2=1$ . The parentheses used for some of the subscripts are for clarity only. By combining Eqs. (42), (43) and (40), we have all the derivatives of the diagonal stress terms.

We use the first two terms in Eq. (17) to obtain the shear derivatives:

$$\delta \mathbf{\Omega} \mathbf{S}^B - \mathbf{S}^B \delta \mathbf{\Omega} = \begin{bmatrix} 0 & \bar{H}_{12}^{(kl)} \frac{S_{11}^B - S_{22}^B}{\lambda_1 - \lambda_2} & \bar{H}_{13}^{(kl)} \frac{S_{33}^B - S_{11}^B}{\lambda_3 - \lambda_1} \\ & 0 & \bar{H}_{23}^{(kl)} \frac{S_{22}^B - S_{33}^B}{\lambda_2 - \lambda_3} \\ \text{Symm} & & 0 \end{bmatrix} \delta \varepsilon_{kl} \quad (44)$$

This gives the variation of the indicated (off diagonal) components of stress as a function of the independent strain component  $kl$  due to the rotation of the eigenvectors. This is the only shear contribution, yielding for Biot strains the result

$$S_{ij,kl}^B = \bar{H}_{ij}^{(kl)} \left[ 2C_1 + 2C_2\psi_{ij} + \frac{p}{\lambda_i\lambda_j} \right] \quad (45)$$

$i \neq j$

The tangent modulus for Green's strains will be shown without proof. Their derivation is done in exactly the same manner as for Biot strains and presents no further difficulties. The equations defining the stress and the pressure are as follows:

$$S_{ii}^G = 2(C_1 - C_2 e_i^{-2}) - \frac{1}{e_i} p \quad (46)$$

$$Dp = 2 \left( C_1 - C_2 \sum_{i=1}^3 v_i^2 e_i^{-2} \right); \quad D \equiv \sum_{i=1}^3 \frac{v_i^2}{e_i}$$

The  $H$  matrices are slightly modified, as are the strain derivatives along the director:

$$\mathbf{H}^{(11)} = \begin{bmatrix} 2 & 0 & 0 \\ 0 & 0 & 0 \\ 0 & 0 & 2\varepsilon_{33,11} \end{bmatrix}; \quad \mathbf{H}^{(22)} = \begin{bmatrix} 0 & 0 & 0 \\ 0 & 2 & 0 \\ 0 & 0 & 2\varepsilon_{33,22} \end{bmatrix} \quad (47)$$

$$\mathbf{H}^{(12)} = \begin{bmatrix} 0 & 1 & 0 \\ 1 & 0 & 0 \\ 0 & 0 & 2\varepsilon_{33,12} \end{bmatrix}; \quad \mathbf{H}^{(23)} = \begin{bmatrix} 0 & 0 & 0 \\ 0 & 0 & 1 \\ 0 & 1 & 2\varepsilon_{33,23} \end{bmatrix}; \quad \mathbf{H}^{(13)} = \begin{bmatrix} 0 & 0 & 1 \\ 0 & 0 & 0 \\ 1 & 0 & 2\varepsilon_{33,13} \end{bmatrix}$$

and

$$b_i \equiv 2\varepsilon_i + 1; \quad B \equiv b_1 b_2 - \gamma_{12}^2$$

$$2\varepsilon_{33,11} = \frac{2}{B} (-b_3 b_2 + \gamma_{23}^2); \quad 2\varepsilon_{33,22} = \frac{2}{B} (-b_1 b_3 + \gamma_{13}^2) \quad (48)$$

$$2\varepsilon_{33,12} = \frac{2}{B} (b_3 \lambda_{12} - \gamma_{23} \gamma_{13}); \quad 2\varepsilon_{33,23} = \frac{2}{B} (b_1 \lambda_{23} - \gamma_{13} \gamma_{12})$$

$$2\varepsilon_{33,13} = \frac{2}{B} (b_2 \lambda_{13} - \gamma_{12} \gamma_{23})$$

Eq. (35) is unchanged, with the remaining quantities required expressed as follows:

$$S_{ii,kl}^G = (4C_2 e_i^{-3} + p e_i^{-2}) \bar{H}_{ii}^{(kl)} - e_i^{-1} p_{,kl} \quad (49)$$

With Eq. (42) unchanged, we use the following to compute the derivative of the pressure term:

$$\Gamma_{,kl} = 4C_2 \sum_{i=1}^3 \left[ v_i^2 e_i^{-3} \bar{H}_{ii}^{(kl)} + v_{i+1} v_{i+2} \bar{H}_{(i+1)(i+2)}^{(kl)} \frac{e_{i+1} + e_{i+2}}{e_{i+1}^2 e_{i+2}^2} \right] \quad (50)$$

and

$$D_{,kl} = - \sum_{i=1}^3 \left[ v_i^2 e_i^{-2} \bar{H}_{ii}^{(kl)} + 2v_{i+1} v_{i+2} \bar{H}_{(i+1)(i+2)}^{(kl)} e_{i+1}^{-1} e_{i+2}^{-1} \right] \quad (51)$$

The reader is reminded of the modular nature of the subscripts in Eqs. (50-51). Finally for the shear terms, we have

$$S_{ij,kl}^G = \frac{\bar{H}_{ij}^{(kl)}}{e_i e_j} \left[ 2C_2 \frac{e_i + e_j}{e_i e_j} + p \right] \quad (52)$$

$i \neq j$

This completes our derivation of the tangent modular matrices for both Biot and Green strain measures. The section on implementation will show that in practice, it is very simple to translate and test these relationships in a simple UMAT that can be run in either the Structural Analysis of General Shells (STAGS)<sup>8</sup> or ABAQUS finite element codes.

### I. Shell kinematic correction

With the development in this section, we have derived stresses and the tangent modular stiffness matrix for solids and shells with and without transverse shear. For membrane response based on a total Lagrangian formulation that may or may not include corotation<sup>1</sup>, all the effects of shell cross section thinning have been taken into account. There is no kinematic constraint on such stretching, and the only limitation is the applicability of the Mooney-Rivlin potential function to the actual physics of the problem. In fact, there is no restriction whatsoever to extending the formulation to other more generalized potential functions, or to other strain measures, such a logarithmic. However, when the contribution of bending energy becomes important, one other correction is required. For shell elements, the (assumed linear) variation of the strain through the thickness depends on the thickness coordinate. Fortunately, most problems where bending dominates have small changes in the shell wall thickness; for almost all problems with significant thinning, the membrane terms dominate the response completely. Unfortunately, should the case apply where the thickness change is important, it is much more difficult to modify the kinematics in the style of UMAT. For STAGS we were able to do the modification in the through-the-thickness integration routine, by computing  $\lambda_3$  and multiplying that by the thickness of the undeformed section before performing the integration. When we ran the examples that follow this section, we saw almost no difference in results, even for the case that has significant bending. The way most finite element software is organized makes the computation of the tangent modular terms that come from thickness modifications very cumbersome. We were able to get good solutions without these small terms.

### III. Implementation Considerations

The strategy common to all elements includes determination of the principal strains and their eigenvectors. Following this operation, we compute the stresses and the tangent modular matrix. Finally, we transform the resulting stresses and the tangent modular matrix back to the original reference system for use by the finite elements. The argument list to UMAT provides all the necessary information for these basic operations except for whether the Green's or Biot strain measure is chosen at the element level. For STAGS, it was a very simple matter to overcome this restriction; we suspect that a similar situation exists for ABAQUS. For solids and shells without transverse shear, the UMAT is quite compact, and was very simple to construct.

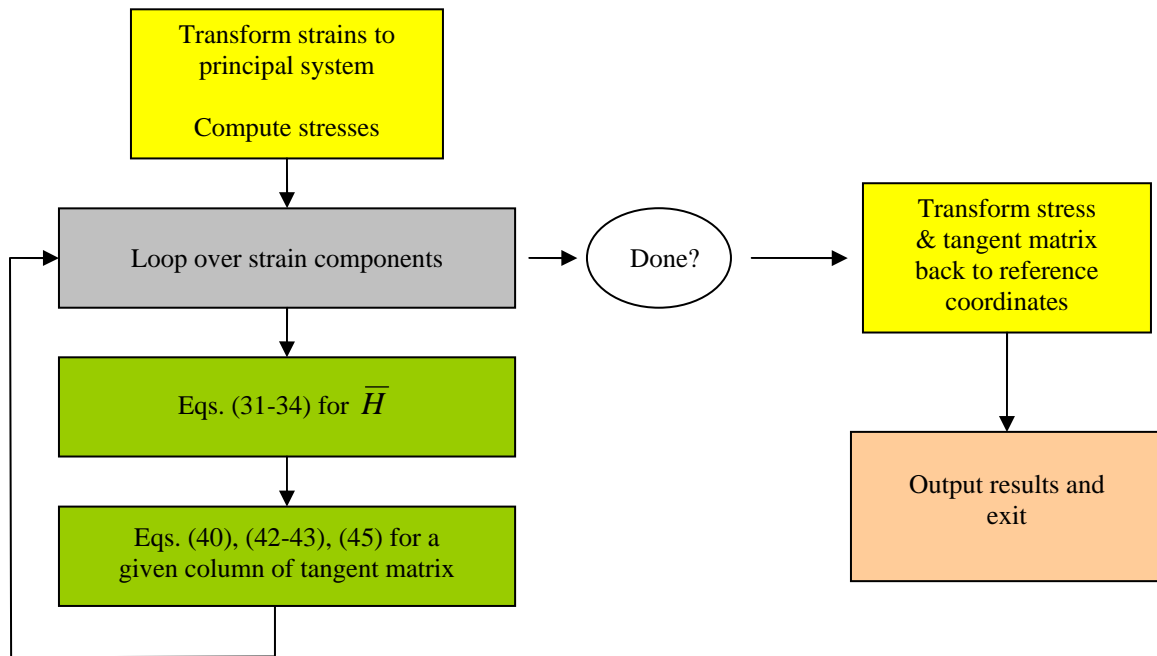


Figure 1. Software organization for shells with transverse shear deformation.

The situation is a bit more complicated for shells with transverse shear deformation. In this case, the stress computation is just as straightforward as before, but the tangent modular matrix requires additional steps. Fig. 1 illustrates the major steps in the procedure. The added complexity comes in the form of a loop over the 5 independent strain components. It turns out, however, that the extra effort is limited to keeping track of the strain indices and applying the equations mentioned in the boxes.

The implementations for all elements were tested using finite difference, with results matching the precision of the finite difference operation itself.

#### IV. Example Problems

##### J. STAGS finite elements

Three shell elements and three solid elements will be mentioned in the results that follow. The following list contains some basic information about each element:

1. E410: an incompatible 4-node C1 shell element based on a cubic transverse displacement field, but linear in the in-plane directions. Available with the nonlinear Green's strain option.
2. E480: an Assumed Natural Strain (ANS<sup>9</sup>) 9-node shell element based on isoparametric quadratic Lagrange interpolation.
3. E330/E430: a triangle based on the work of Madenci<sup>10</sup>.
4. E881 & E883: 8 & 27 node ANS solid brick elements<sup>11</sup>.
5. E885: an isoparametric 20 node "Serendipity" element. Available with Green's strain nonlinear option.

##### K. List of example problems

We present the following example problems to demonstrate the effectiveness of our UMAT software:

1. A constant "extrusion" demonstrating equal performance of shell and solid idealization for plane stress response.
2. A constrained "extrusion" case
3. The Ogden<sup>12</sup> rubber disk (ABAQUS benchmark problem 1.1.7<sup>13</sup>).
4. The Yamada & Kikuchi<sup>14</sup> indentation problem.
5. Bending of a hexahedral block.

##### L. "Plane stress" extrusion

The following example compares the response of brick elements and shell elements for a plane stress, uniform extrusion problem:

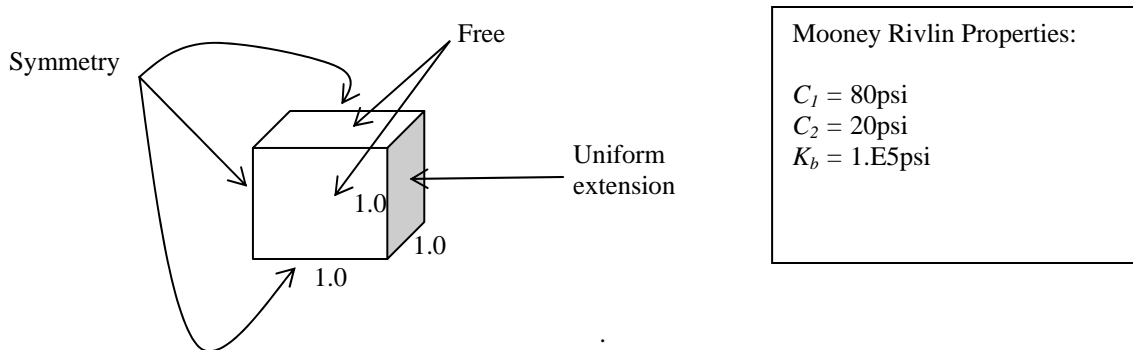


Figure 2. Uniform extrusion that doubles the length of a unit cube.

The boundary conditions allow the two free sides to contract uniformly in response to a unit extension of the free edge (shaded). The three hidden faces are symmetry conditions, as shown. We performed three analyses:

1. Biot strain, E881 brick element.
2. Biot strain, E410 shell element
3. Green strain, E410 shell element

All runs produced identical response, with data summarized in Table I:

**Table I: Extrusion test case response.**

	Lateral Contraction	Strain	End Reaction Force
E881 Brick	.29285	1.0	315 (lbs)
E410 Shell	.29289	1.0	315
E410 Shell (Green's)	.29289	1.5	315

One can see that the response for all three runs is identical, including the lateral contraction. Although Green's strain is numerically larger, the forces generated are exactly the same. Even though the shell kinematics are very different from those of solids, with the constant volume and zero stress constraints applied explicitly, the response of the shell element is identical to the solid brick element.

### M. Constrained Extrusion

This case illustrates a plane-stress response, but this time with lateral motion restrained at one end:

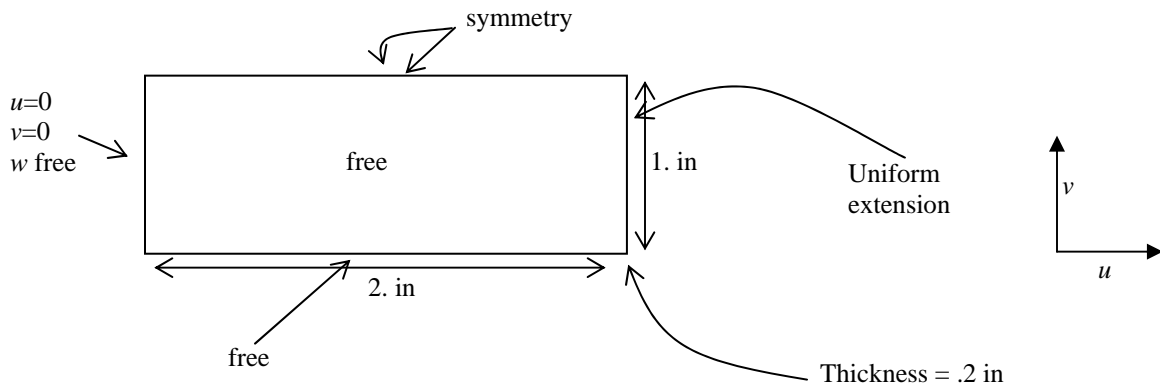
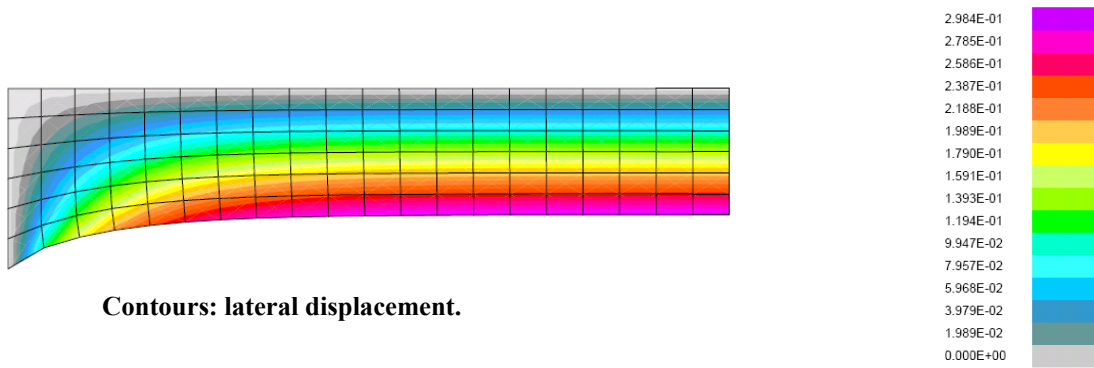


**Figure 3. Constrained extrusion case geometry.**

For solid element models, the top surface is free and the bottom is “symmetry,” as shown above; this corresponds to the plane-stress conditions used in the shell models. The plate was loaded by a uniform end extension of 2 inches. Again, both solid and shell element yielded almost identical results, with the same reactions and deflected shapes. We ran E410, E885 (Serendipity 20 node brick), E883 (27 node ANS brick), and E881. Where applicable, results for Biot strain were compared to Green strain, with identical reaction forces and identical displacements. The deflected shape is illustrated in Fig. 4. This is the first example where there is local rotation of individual elements, and where the strains vary. It is comforting to know that for six separate analyses using two strain measures and four elements we obtained identical lateral displacements as a function of position, and the same reaction force of 64.29 lbs. The material properties are identical to the preceding problem. Figure 5 shows just how close the match is for the lateral deflection as a function of distance along the free edge of the plate.



Contours: lateral displacement.

Figure 4. Constrained extrusion case response.

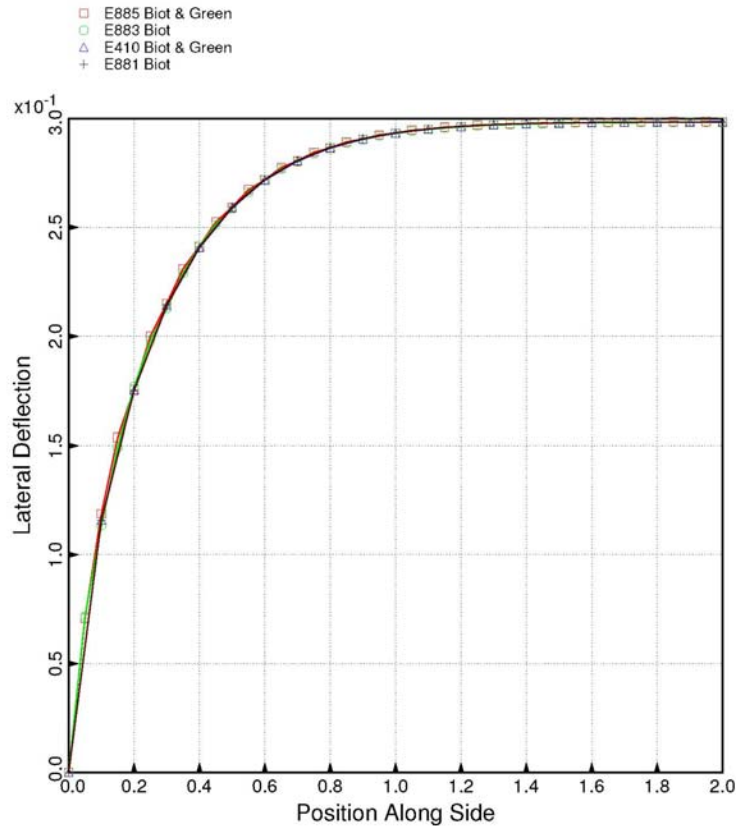
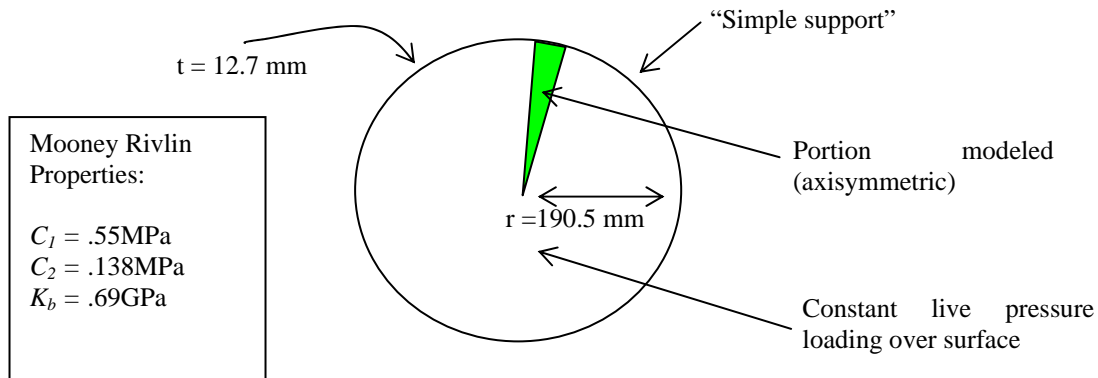


Figure 5. Comparison of response of various elements and strain measures.

**N. Response of rubber disk to live pressure load**

The problem chosen here is taken from ABAQUS<sup>13</sup> to be used as a benchmark for hyperelastic response for strains of the order of 400% or more. Two disk thicknesses are analyzed in Refs. 13 and 15, but the thicker disk we chose is by far the most challenging for shell elements. The model is described in Fig. 6 below. This example poses a severe test to both our solid and shell elements, for different reasons. For shell elements, significant thinning of the disk exercises our implementation of the constant volume and zero stress constraints. For solids, the response is very sensitive to the bulk modulus, hence convergence problems are to be expected. For the E881 solid, we were able to satisfy the volume constraint exactly at the centroid by treating the pressure as a Lagrange constraint and solving for

the pressure indirectly, by the method of Felippa<sup>16</sup>. This method alters the solution sequence of operations to include a second evaluation of the internal force vector and a method to update the value of the pressure Lagrange multiplier; it was extremely simple to implement that algorithm into STAGS. For other elements, we did not attempt to account for incompressibility except by using a large bulk modulus. In Fig. 7 we find the normal deflection of the center of the disk plotted as a function of pressure for all the elements mentioned above. The busy nature of the plot testifies to the almost exact agreement every element had with the ABAQUS benchmark and Ogden's<sup>12</sup> results, clearly demonstrating the capability of the methods used here. One will notice that there are two curves for the E881 solid element case; one curve is for the top surface, and the other is for the bottom. They do not match because the cross section thins enough for the difference to be seen on the plot.



**Figure 6. ABAQUS benchmark disk problem.**

There were a few problems, however. The E883 and E885 solid elements were slow to converge because we had to use such a large bulk modulus to get volume-conserving results; hourglassing took place if we enforced the volume constraint only at the centroid. The E885 20 node solid was especially vulnerable, with locking or hourglassing depending on whether we applied the bulk modulus at all integration points or only at the centroid. We included two curves of this element to demonstrate just how sensitive it is to the bulk modulus. The lower curve is response of the top surface for the bulk modulus stated in Fig. 6; the upper curve is the same response for a bulk modulus one order of magnitude higher. These are problems particular to a given element that were not tackled here. The E410 Green, E410 Biot, and E330 Biot formulations converged at about the same rate, yielding excellent results in the fewest load steps. This problem shows that our methods are capable of computing very large strain >400% response within a total Lagrangian framework and using standard, off-the-shelf (actually rather antique) finite elements. To see just how extreme this case is, we ran a quarter model so we could plot a picture, shown in Fig. 8.

Finally, the reader will notice that the E883 ANS element is not included in this example because up to the present time, we were not able to overcome locking that results from a large bulk modulus and its full 3x3x3 integration.

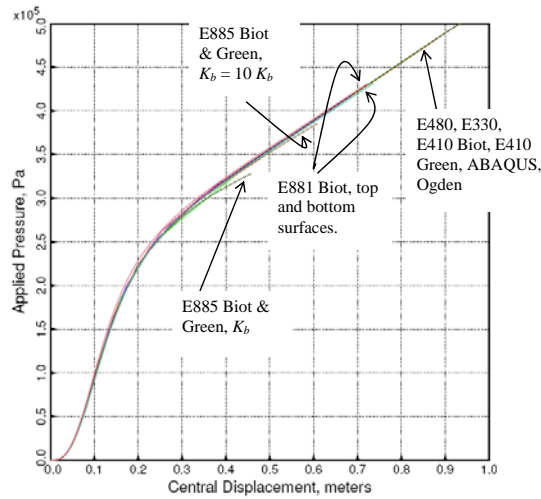


**Figure 7. Response of pressure-loaded disk.**

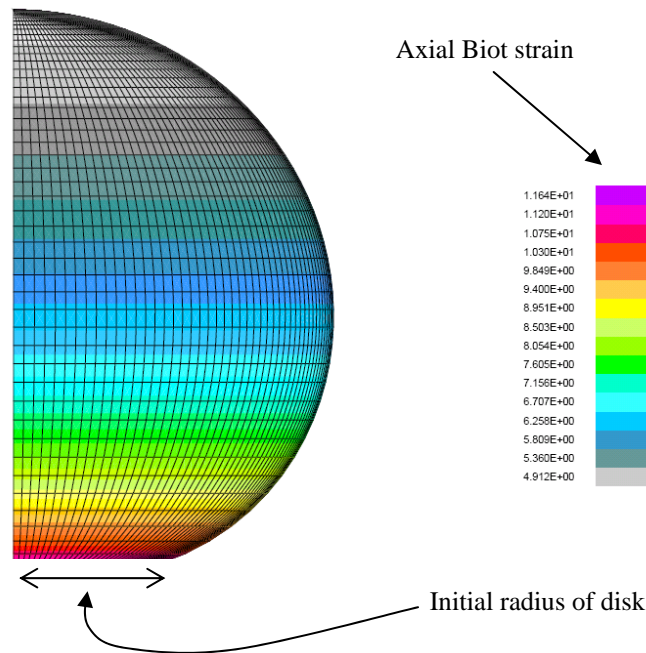


**Figure 8. Final deformed shape of inflated rubber disk.**

**O. The Yamada Kikuchi indentation problem**

This problem tests our methods with a plane-strain response that includes very large material strains and rotations. Originally due to Yamada & Kikuchi<sup>14</sup> and also found in Refs. 5-7, this problem consists of a rectangular block with a uniform indentation on its left top half, allowed to slide but otherwise restrained on three edges, and free on its top right half, as shown in Fig. 9. The imposed displacement boundary condition requires careful consideration. In our results, displacements parallel to the loaded edge (heavy black line) are permitted. This boundary condition is not the same as having a heavy steel plate push on the material and allowing the material to

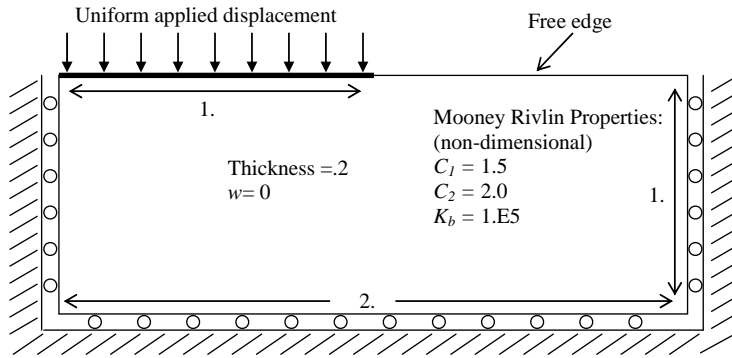


**Figure 9. Indentation plane strain problem**

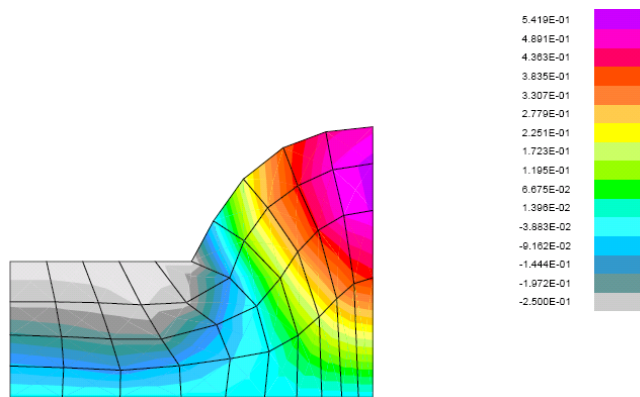


**Figure 10: Response of indentation problem, coarse grid.**

squeeze out. Rather, it means the nodes are free to move along the edge, which also allows the loaded section itself to expand or contract. The boundary condition is the same as the one used by Moita<sup>6</sup>, which for a rather coarse grid like the one he used is displayed in Fig. 10. The element in this picture is a plane-strain form of the E410, with our solid elements giving essentially the same results. Colors represent vertical displacements, and as in our previous examples, deformed shapes are not scaled. The reader will note the strong similarity with Fig. 14 in Ref. 4. To get a better understanding of this problem, we conducted a mesh refinement study using the total reaction force on the loaded segment as the measure of convergence. Figure 11 summarizes a series of analyses with two solid elements and two strain measures. Clearly convergence is slow, as would be expected if response in the area adjacent to the loaded edge (where strains vary significantly over a very short range) determines convergence. Figure 12 shows an example of a much finer grid and the huge distortions near the reentrant corner. We had serious problems with ill-conditioning and locking, especially for the E410 which became useless for the finer mesh models. Although we were able to extend the utility of the E881 brick by applying the bulk modulus term to the centroid only and using the method in Ref. 16, doing the same thing for E885 caused hourglassing, just as in the ABAQUS disk. However, as in previous examples, these are element kernel details not germane to the methodology developed here.

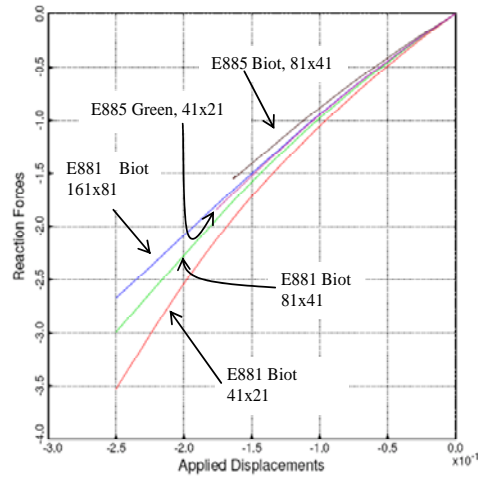


**Figure 11. Comparison of reaction force as a function of mesh density.**

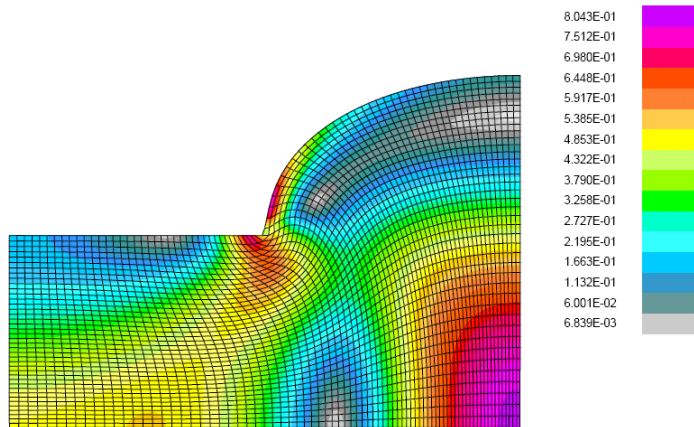


**Figure 12. First principal strain for the 81 x 21 E881 mesh (Biot strain).**

### **P. Bending of a hexahedral block**

This final example demonstrates behavior unsuitable for shell elements because the strain is far from linear as a function of the distance along the thickness direction. We are, however, able to show the effects of the volume constraint and significant transverse shear deformation as the block deforms. The geometry and boundary conditions are shown in Fig. 13. As one can see here, this is quarter model of a block 2 x 1 x .5 units long. The tractions are allowed to vary slightly along the thickness direction (see formula in Fig. 13, where  $z$  is in the thickness direction) to induce an initial normal deflection that will increase in response to the axial loading, as would be found in the elastica problem. The material properties are identical to the previous example (Fig. 9). In this analysis we used only the E881 solid element with the volume constraint imposed exactly at the centroid of each element.

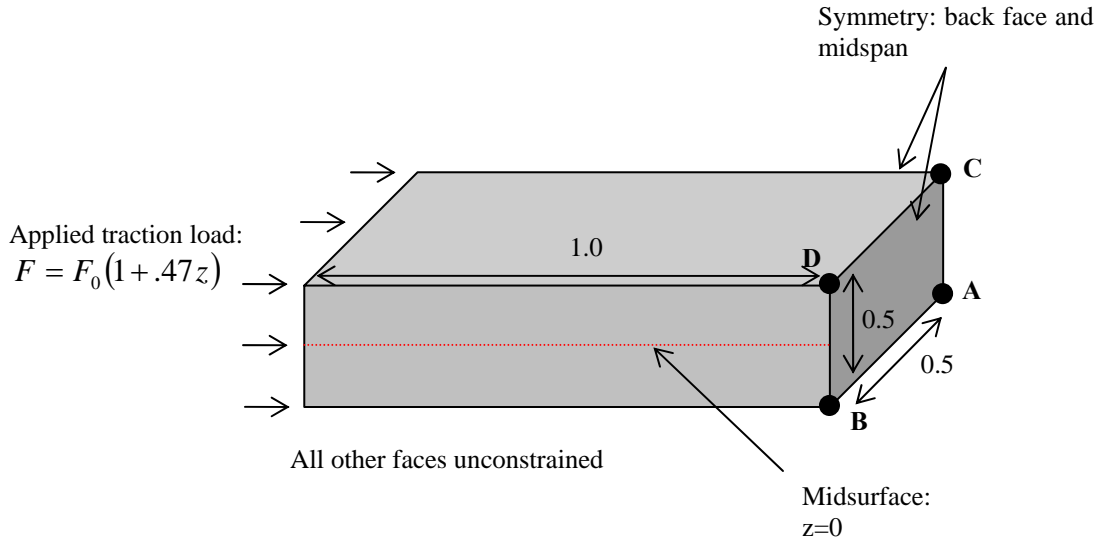


**Figure 13. Geometry, loading, and boundary conditions of hexahedral block.**

We carried the analysis beyond the point of maximum normal deflection, yielding the following final configuration, as shown in Fig. 14.

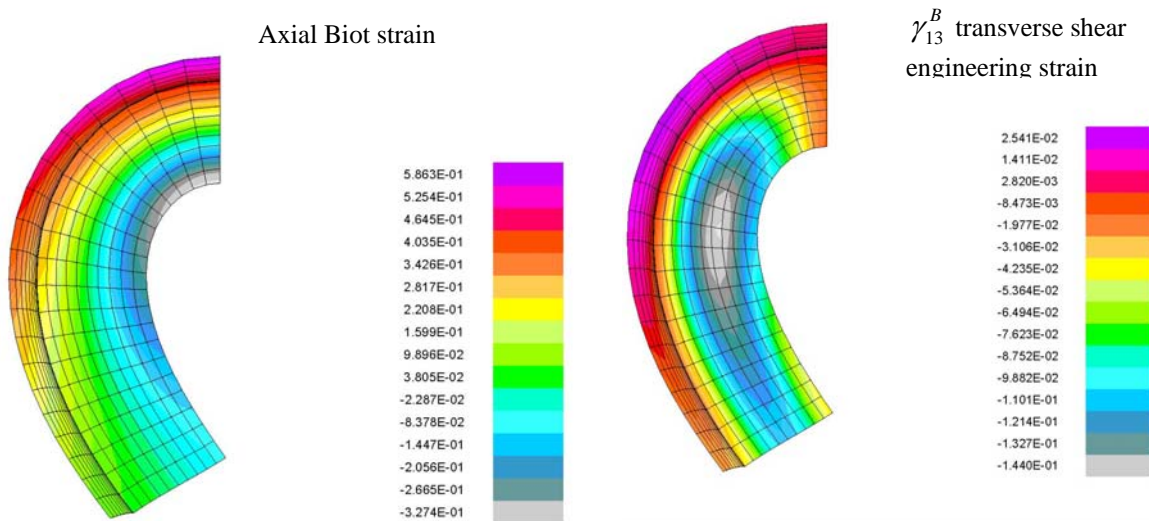


**Figure 14. View from axial symmetry plane showing strains.**

This particular view is directly out from the axial (long) symmetry plane that coincides with the plane of the paper. One of the things the reader will notice is the flaring out of the section as one moves away from the symmetry plane. Another feature is the very large axial strain of over 58%. As expected, the transverse shear is very significant, especially in the center of the segment. Figure 15 shows a sequence of responses to increasing load, but this time looking from the free loaded end toward the symmetry plane at the midspan; since this symmetry boundary coincides with the plane of the figure, the deformation there is confined to that plane. In both Figs. 14 and 15, the deformation is not exaggerated, and therefore represents the physical appearance of the block.

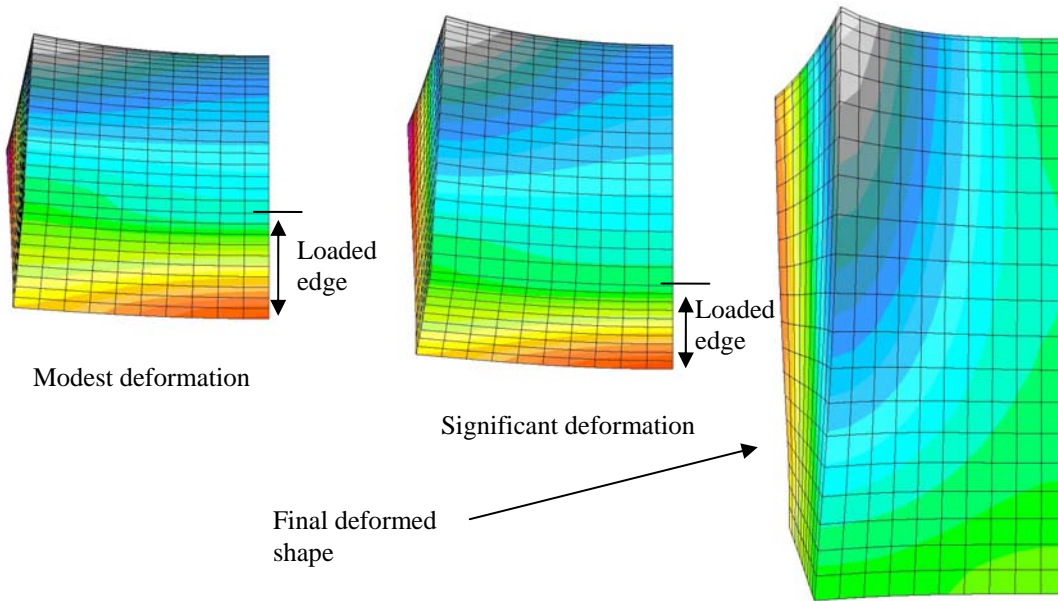


Figure 15. Looking along axial direction toward midspan, showing  $\epsilon_{22}^B$  strain distribution.

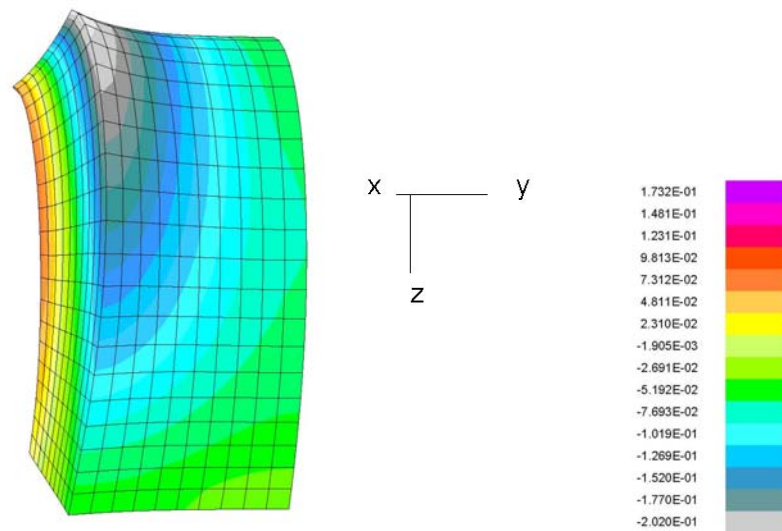
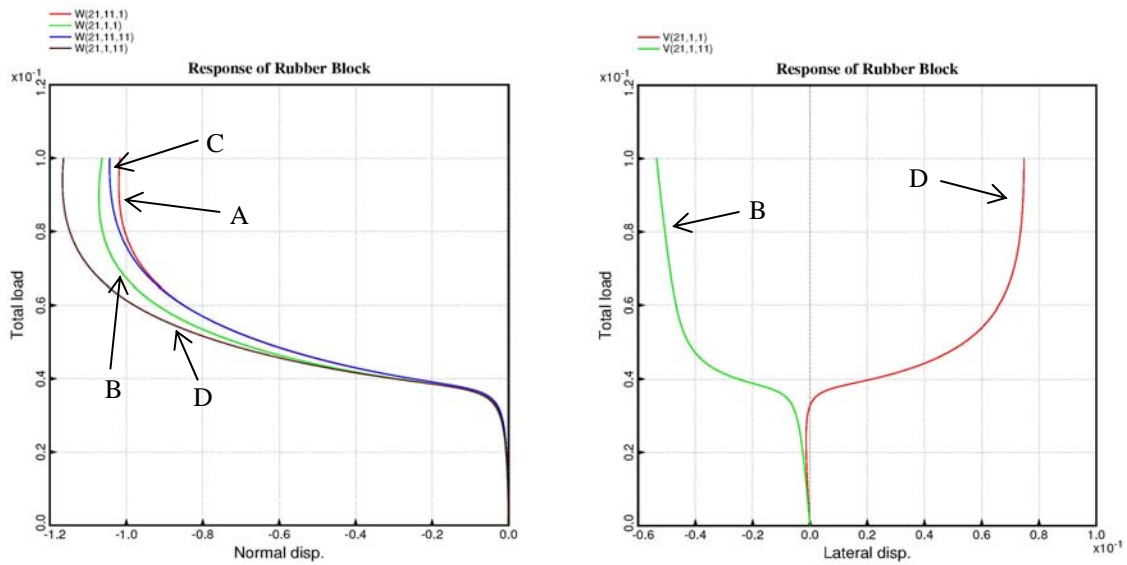


Figure 16. Expanded view of final configuration showing  $\epsilon_{22}^B$

The reader will note the “squashed” elements near the symmetry plane; they appear that way because the viewer’s perspective is almost tangent to these elements. It is very clear that there is huge distortion in the plane of the midspan. Finally, in Fig. 16 we show an expanded view of the final configuration with the figure tilted slightly to the right; this view offers an improved perspective of the deformation.



**Figure 17. History plots of displacements at midspan symmetry boundary.**

Figure 17 gives further insight into the response by showing a history of the deflection of the four labeled points in Fig. 13. In that figure, the reader will see four darkened circles with letter labels, each of which corresponds to one of the traces labeled with the same letters in Fig. 17. Two features stand out in these plots. First, the response has the characteristics of sudden buckling that occurs at a total axial load of about .38. The onset is gradual because of the small moment imposed on the beam. Before buckling, the compression of the block causes it to expand uniformly in both the lateral and transverse directions. This is illustrated by the small negative transverse displacements of both curves on the second (right side) plot. Immediately after the buckling, the beam bends and the side with the compression flares out (here, negative lateral displacements), and on the tensile side, positive (inward) deflections. The beam also curls, as shown on the first plot. Along the line AB, the transverse displacements begin to diverge because of this curling. Likewise, similar behavior is revealed along line CD. Similarly, compression forces the beam to thicken at point A, and thin at point C, resulting in the difference shown by their respective curves. Most all of this behavior stems from the volume constraint accompanied by large transverse shear strains, all of which can be seen in Figs. 14-16.

## V. Summary and Conclusions

In this paper we completed what we started in Ref. 1, where we demonstrated that corotation based on irrotational deformation at the element centroid yields an excellent approximation to the Biot strain measure when the basic element kernels possess a simple linear strain-displacement relationship. In that earlier paper, we demonstrated the efficacy of the method for several example problems involving large strain. Here we presented the details of a straightforward material model definition based on the Mooney-Rivlin potential function suitable for a UMAT implementation. The model applies equally well to plane-stress shell-element or solid-element response. The examples herein show just how well the method works. We also showed in the examples that both the Green or Biot strain measures yield identical responses, confirming that the material model is correctly derived from the strain energy potential function. It is clear from the way the material model is derived that the method can be extended to any number of more general potential functions, or other strain measures if so desired. Biot and Green's strain are of course suitable strain measures for more complex material behavior, including large scale plastic deformation.

## References

1. C. Rankin, "Application of Linear Finite Elements to Finite Strain Using Corotation," presented at the 47<sup>th</sup> AIAA/ASME/ASCE/ASC Structures, Structural Dynamics, and Materials Conference, AIAA paper # AIAA-2006-1751 (2006).
2. Rankin and Brogan, "An element-independent co-rotational procedure for the treatment of large rotations," *ASME J. Pressure Vessel Techn.* Vol. 108 (1986) pp. 165-174
3. Rankin and Nour-Omid, "The use of projectors to improve finite element performance," *Comput. & Structures* Vol. 30, (1988) 257-267
4. Nour-Omid and Rankin, "Finite rotation analysis and consistent linearization using projectors," *Compt. Meths. in Applied Mechanics and Engng.* Vol. 93 (1991) pp. 353-384.
5. Crisfield, M. A., *Non-linear Finite Element Analysis of Solids and Structures – Vol. 2 Advanced Topics*, Chapter 13. John Wiley & Sons, Inc., New York (1997).
6. Moita, G. F. & Crisfield, M. A., "A Finite Element Formulation for 3-D Continua Using the Corotational Technique," *Int. J. for Numerical Meth. In Engn.*, vol. 32, pp3775-3792 (1996).
7. Crisfield, M. A., *Non-linear Finite Element Analysis of Solids and Structures – Vol. 2 Advanced Topics*, Chapter 18. John Wiley & Sons, Inc., New York (1997).
8. Rankin, C. C., Brogan, F. A., Loden, W. A., Cabiness, H. D., "STAGS User Manual – Version 5.0," Rhombus Consultants Group, Inc., Palo Alto, CA, revised January 2005 (on-line). Previously Report No. LMSC P032594, Lockheed Martin Missiles and Space Company, Palo Alto, CA.
9. Stanley, G. M., "Continuum-Based Shell Elements," PhD Dissertation, Dept. of Mechanical Engineering, Stanford University (1985).
10. Madenci, E. & Barut, A., "A free-formulation-based flat shell element for non-linear analysis of thin composite structures," *Int. J. of Num. Methods in Engineering*, Vol. 37, pp. 3825-3842 (1993).
11. K. C. Park, E. Pramono, G. M. Stanley, and H. A. Cabiness, "The ANS shell elements: Earlier developments and recent improvements." In Ahmed K. Noor, Ted Belytschko, and Juan C. Simo, editors, *Analytical and Computational Models of Shells*, pp. 217-239. American Society of Mechanical Engineers, New York, N.Y. (1989).
12. Ogden, J. T., *Finite Elements of Nonlinear Continua*, McGraw-Hill (1972)
13. ABAQUS 6.4 Benchmarks Manual, Section 1.1.7.
14. Yamada, T. & Kikuchi, F., "An Arbitrary Lagrangian-Eulerian Finite Element Method for Incompressible Hyperelasticity," *Comput. Methods in Appl. Mech. Engng.*, Vol 102, pp149-177 (1993).
15. Hughes, T. J. R., and E. Carnoy, "Nonlinear Finite Element Shell Formulation Accounting for Large Membrane Strains," *Nonlinear Finite Element Analysis of Plates and Shells*, AMD, vol. 48, pp. 193-208 (1981).
16. Felippa, C. "Iterative Procedures for Improving Penalty Function Solutions of Algebraic Systems," *Int. J. Num. Meth. In Engng.*, **12**, pp 821-836 (1978)